

Cantilever dynamics in atomic force microscopy

Dynamic atomic force microscopy, in essence, consists of a vibrating microcantilever with a nanoscale tip that interacts with a sample surface via short- and long-range intermolecular forces. Microcantilevers possess several distinct eigenmodes and the tip-sample interaction forces are highly nonlinear. As a consequence, cantilevers vibrate in interesting, often unanticipated ways; some are detrimental to imaging stability, while others can be exploited to enhance performance. Understanding these phenomena can offer deep insight into the physics of dynamic atomic force microscopy and provide exciting possibilities for achieving improved material contrast with gentle imaging forces in the next generation of instruments. Here we summarize recent research developments on cantilever dynamics in the atomic force microscope.

Arvind Raman*, John Melcher, and Ryan Tung

Birck Nanotechnology Center and the School of Mechanical Engineering Purdue University, West Lafayette, IN 47907, USA

*E-mail: raman@purdue.edu

Since the invention of the atomic force microscope (AFM)¹, dynamic atomic force microscopy (dAFM) has become one of the most important tools in nanotechnology with its unmatched capabilities of: (i) measuring topography and physico-chemical properties of organic and inorganic materials at nanometer length scales in a variety of ambient media; and (ii) the manipulation and fabrication of a variety of functional nanostructures. Moreover, in dAFM materials are probed with gentle forces by means of an oscillating nanoscale tip that intermittently interacts with the sample. These capabilities have propelled dAFM into a leading tool that allows the experimentalist to directly 'see' and 'touch' at the nanoscale.

Broadly speaking, dAFM can be classified into frequency modulation² (FM) AFM – also known as noncontact AFM – and amplitude modulation³ (AM) AFM – also known as tapping-mode or intermittent contact AFM. In FM-AFM, the phase of oscillation and tip amplitude are held constant by means of feedback circuits, while in AM-AFM the drive frequency is held constant and the tip amplitude is maintained constant by means of active feedback. This article focuses mostly on cantilever dynamics in AM-AFM.

The interest in the dynamics of AFM, especially its nonlinear aspects, initially grew out of observations of instabilities in dAFM that occur at certain oscillation amplitudes⁴. A deeper understanding of cantilever dynamics is becoming increasingly important in two of the

biggest growth areas of dAFM: (i) the manipulation and imaging of soft matter, especially in biology; and (ii) the accurate quantification of sample properties in materials science. This requires the development of a new generation of AFM with greatly reduced imaging forces and improved material contrast. In moving toward this major goal in dAFM, a number of research groups and companies are devoting considerable research efforts to control, tune, or exploit cantilever dynamics to reduce imaging forces and develop new modes to improve material contrast and sensitivity. The purpose of this article is to review these latest developments in cantilever dynamics in the AFM and present an outlook of the future of these developments in the next generation of dAFM.

Eigenmodes of AFM cantilevers

AFM microcantilevers are fabricated from single-crystal Si or Si_3N_4 , and possess a sharp conical or pyramidal tip near their free end with which to probe the sample surface. Just like a taut string possesses many eigenmodes of vibration each with its own natural frequency, so too do AFM microcantilevers. The intent of any dAFM system is to drive the microcantilever externally into a resonance of a specific eigenmode. Thus, it is instructive to understand what the eigenmodes of AFM microcantilevers are and how they are used in dAFM.

In Fig. 1, three AFM microcantilevers are shown including (a) a stiff rectangular cantilever (~50 μm long), (b) a soft rectangular cantilever (~290 μm long), and (c) a soft triangular cantilever (~125 μm long) for biological applications in liquids. As can be seen, the vibration spectrum contains distinct peaks corresponding to the mechanical resonances of the cantilever or of the dither piezo; under ambient conditions, the quality (Q) factors of the microcantilever resonances are usually much larger than those of the piezo resonances, thus allowing one to distinguish between those peaks.

The main eigenmodes consist of bending modes (denoted B1, B2, etc.) transverse to the plane of the cantilever and the torsion modes (denoted T1, T2, etc.) where the T_n or B_n mode ($n = 1, 2, \dots$) contains $n-1$ vibration nodes along the axis of the cantilever. However, sometimes the lateral bending modes L1, L2, etc. can also be observed where the cantilever bends in its plane laterally. The greater the mode number, the larger the resonance frequency and Q -factor and the greater its spatial modulation.

When a microcantilever eigenmode is excited by tuning the drive frequency to the eigenmode's natural frequency, the tip motion should oscillate harmonically, like clockwork, with a well-defined motion. If a bending mode B_n ($n = 1, 2, \dots$) is excited, ideally the sharp tip should oscillate perpendicular to the surface, while if one of the torsion modes T_n ($n = 1, 2, \dots$) is excited, then the tip should oscillate tangentially to

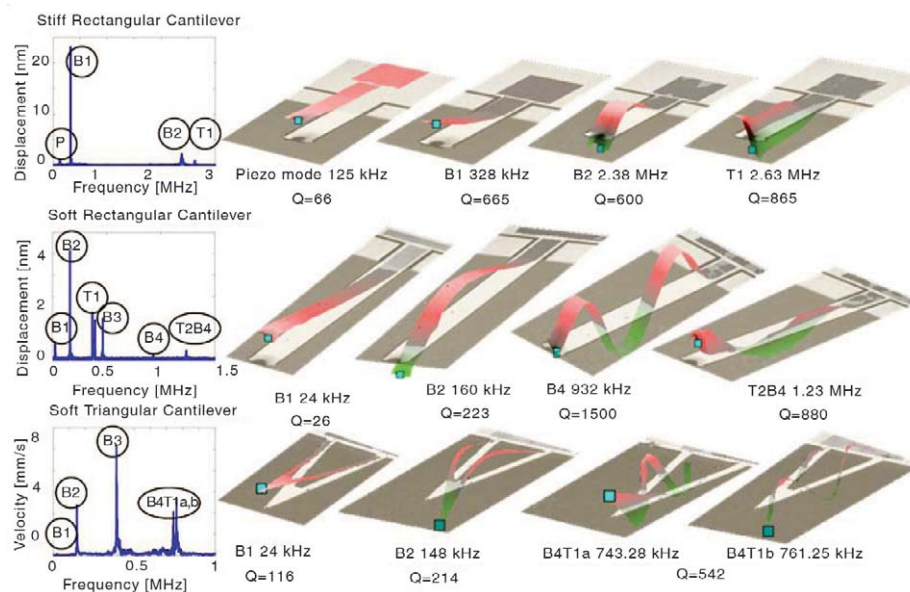


Fig. 1 Experimentally measured operating deflection shapes (ODS) or eigenmodes of several AFM cantilevers. Each cantilever chip was mounted onto a dither piezo, excited, and scanned with the Polytec MSA400 system. The plots show the measured vibration spectrum corresponding to the blue square on the cantilever shown on the right. The nomenclature used denotes the type of resonance and the mode number corresponding to that resonance, e.g. B1 represents the first bending mode, T1 represents the first torsion mode. Note that the piezo resonance denoted P, observed in the spectrum of the tapping mode lever, is clearly indicated by the excessive base motion and small relative motion between the tip and base. Some eigenmodes couple the torsion and bending motions, such as in the T2B4 peak for the force modulation lever and the B4T1a,b peaks for the triangular cantilever. Sometimes the lateral bending modes L_n ($n = 1, 2, \dots$) where the cantilever vibrates laterally in its plane couple to torsion motions and the coupled lateral-torsional modes are denoted as LT modes. For rectangular cantilevers, such eigenmodes often arise when (i) the resonance frequencies of a torsional and bending (or lateral) mode are closely spaced and (ii) the tip mass located eccentrically with respect to the cantilever axis couples these motions. On the other hand, for triangular cantilevers, asymmetry between the two arms of the triangle can cause the two peaks (B4T1a,b) representing coupled bending-torsion modes where the vibration is localized in one of two arms.

the sample surface. For the most part, the eigenmodes and resonance frequencies of rectangular AFM microcantilevers can be predicted using simple Euler–Bernoulli beam theory modified to account for the tip mass⁵. However, as shown in Fig. 1, some eigenmodes actually couple torsional and bending motions or torsional and lateral motions^{5–7}. Such coupled modes are denoted as bending–torsion (BT) or lateral–torsional (LT) modes (Fig. 1). If such coupled modes are excited, the tip moves both tangentially and normally to the sample surface.

There has been a surge of interest in these higher modes of AFM microcantilevers, especially in the development of new imaging modes. For instance, in torsion mode or shear force AFM^{8–12}, a pure torsional or lateral bending mode of the AFM cantilever is excited ensuring that the tip oscillates tangentially to the surface. This mode enables the measurement of lateral force gradients, frictional contrasts at the nanoscale, and can also be used for imaging purposes. On the other hand, higher order bending modes are also gaining significant interest because their Q -factors are very high (Fig. 1) and their dynamic stiffness^{8,13–16} is also very high. Consequently, it becomes possible to drive a tip with very small amplitudes, comparable to the decay length of short-range forces, which in turn enables atomic-scale resolution.

Mathematical simulations of cantilever dynamics

When an oscillating AFM microcantilever is brought close to a sample, the tip–sample interactions greatly influence the cantilever dynamics. Realistic tip–sample interaction force models are critical for accurate simulation of the interaction of AFM cantilevers with samples. A variety of tip–sample interaction force models are available, from the Lennard–Jones model to continuum-based models to force models based on *ab initio* molecular dynamics or quantum mechanics simulations¹⁷. In particular, the Derjaguin, Müller, and Toporov (DMT) continuum model¹⁸ is often used to simulate dAFM for stiff samples with low adhesion and small tips. The DMT model considers noncontact van der Waals forces and Hertzian contact forces.

Models governing the dynamics of AFM cantilevers generally involve one of two simplifications: (i) assuming that the cantilever bends as if a static point load is being applied at the cantilever’s free-end and using the corresponding static stiffness to derive a single degree of freedom point-mass model^{19–23}; or (ii) discretizing the classical beam equation based on its eigenmodes leading to either single or multiple degrees of freedom models^{24–31}. While the former approach is incapable of modeling higher flexural modes, nonunique modal masses and stiffnesses have been reported in the latter approach, which is cause for concern^{19, 32–34}. As described by Melcher *et al.*¹⁶, unique *equivalent masses* and *stiffnesses* can be systematically determined by equating the kinetic energy, potential energy, and virtual work of a continuous probe to that of an appropriate point-mass model (Fig. 2). The resulting equation of motion for a base-excited cantilever may be written as:

$$M_{eq}^i \ddot{q} + (M_{eq}^i \omega_j / Q_j) \dot{q} + K_{eq}^i q = F_{ts} + K_{eq}^i y_{eq}^i \quad (1)$$

where F_{ts} is the tip–sample interaction force, q is the tip deflection (with dots representing time derivatives), M_{eq}^i , K_{eq}^i , and y_{eq}^i are the equivalent mass, stiffness, and excitation, respectively, and Q_j is the experimentally observed quality factor for the i^{th} bending mode. Eq 1 forms the basis of most mathematical simulations of dAFM, and assumes that while higher harmonics of excitation frequency may be present in the cantilever vibration, one dominant eigenmode is sufficient to describe the cantilever’s dynamic motion²⁸. As will be described later in this article, there are situations where this assumption no longer holds.

Mathematical simulations of eq 1 are frequently used to study the dynamics of the AFM tip as it approaches or retracts from a sample. Through such simulations, researchers have investigated attractive and repulsive regime oscillations³⁵, power dissipation processes^{36,37}, capillary forces^{38,39}, and peak interaction forces³⁴. Cantilever dynamics also influence images taken using dAFM. Scanned images in dAFM are actually a cumulative result of several effects related to the cantilever dynamics, tip–sample interaction forces, and controller dynamics^{40,41}. When the mathematical model in eq 1 is appended with a model of a lock-in amplifier and a feedback control law, mathematical simulations of the scanning process can be performed. Such simulations help in the interpretation of scanned images and image artifacts^{42–44}. From a broader point of view, cantilever dynamics in dAFM are quite nonintuitive. Where intuition fails, mathematical simulations can provide a valuable insight into the cantilever dynamics and tip–sample interactions.

While the benefits of simulations in dAFM are legion, accurate simulation tools for dAFM are inaccessible to most experimentalists. Recently, a suite of such freely accessible, high-fidelity, research-grade simulation tools for dAFM called VEDA: *Virtual Environment for Dynamic AFM* has been deployed on the nanoHUB (www.nanohub.org) – the web portal for the Network for Computational Nanotechnology (NCN). VEDA simulations (Fig. 3) are run off the national teragrid or other

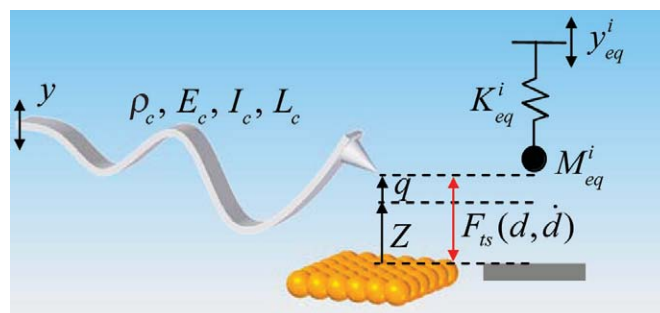


Fig. 2 Equivalent point-mass representation of a continuous AFM cantilever oscillating in a single eigenmode. The continuous cantilever is characterized by linear mass density, ρ_c , elastic modulus, E_c , area moment, I_c , and length, L_c . The corresponding point-mass model is characterized by equivalent stiffness, K_{eq}^i and mass M_{eq}^i . For acoustic excitation, the continuous cantilever is given a base motion, y , while the point mass observes an excitation y_{eq}^i . Finally, the tip deflection, q , and the influence of tip–sample interaction forces, $F_{ts}(d, \dot{d})$ are identical in both models.

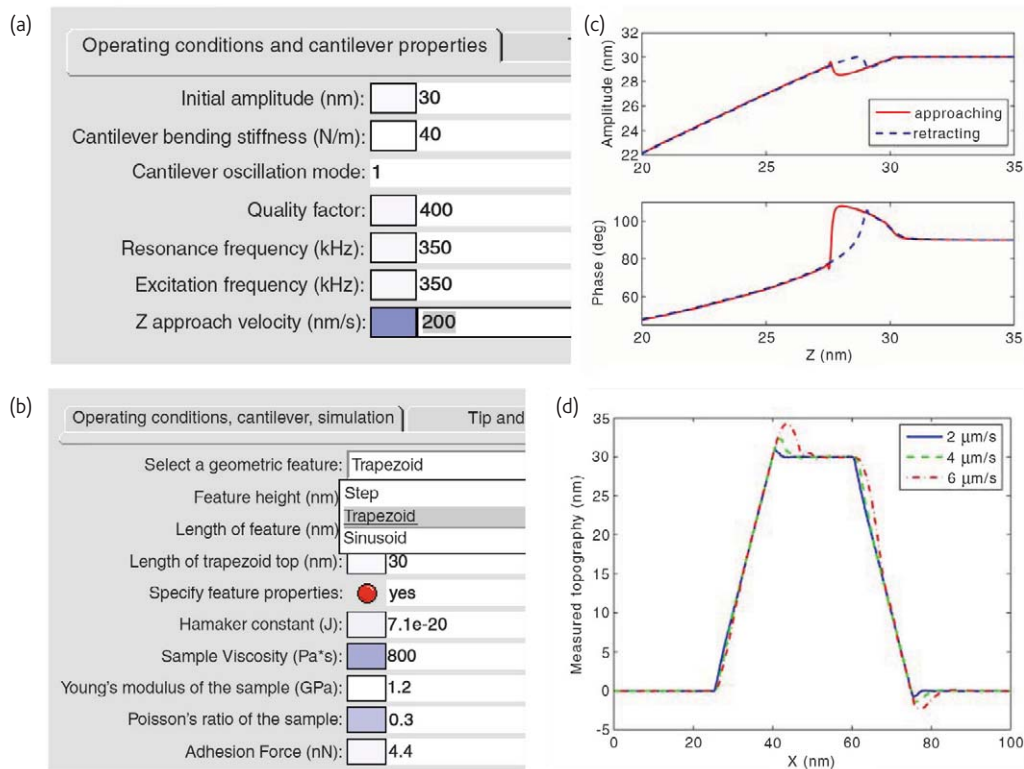


Fig. 3 Overview of VEDA (now available on www.nanohub.org). VEDA accurately simulates probe tip dynamics in dAFM and currently includes two simulation tools for dAFM: a dynamic approach curves (DAC) tool, which simulates an AFM probe excited near a resonance and approaching/retracting from a sample, and an amplitude modulated scanning (AMS) tool, which simulates closed-loop scans over heterogeneous samples in tapping mode. Both tools have been developed for ambient conditions with DMT interaction models, but VEDA will soon expand to include liquid environments, more complex interaction forces, and eventually molecular dynamics simulations. Snapshots from the graphical user interface (GUI) are shown for (a) the DAC tool and (b) the AMS tool. (c) A DAC simulation of the amplitude and phase of a Si AFM probe while approaching (bold) and retracting from a soft sample surface demonstrating attractive and repulsive regimes of oscillation consistent with the published literature⁷⁶. (d) Measured topography of a Si feature simulated by the AMS tool for different scanning speeds.

large computing clusters. To access VEDA, users need only register on nanoHUB, and search for and launch the VEDA tools[‡].

Nonlinear dynamics and chaos

The cantilever dynamics in AM-AFM are highly nonlinear because typical tip oscillation amplitudes (>5 nm) are larger than the decay lengths associated with short-range interaction forces (<1 nm). Thus, cantilever dynamics cannot be predicted by linearizing interaction forces about an equilibrium position.

Early studies⁴ on the dynamics of oscillating AFM tips near a surface show an interesting hysteresis in both the amplitude and phase response as the drive frequency is increased and then decreased across the cantilever's resonance. Later, it was observed experimentally²¹ that the same hysteresis is found when a cantilever approaches and then retracts from a surface at a fixed drive frequency. It has been proposed²¹ that this behavior is the result of a transition between two stable oscillation regimes of the microcantilever.

[‡]The tools are supplemented by a well-documented user manual, as well as learning modules and tutorials in breeze format. At the time of publication, more than a thousand VEDA jobs have been run.

Subsequent studies have attempted to explain this phenomenon in terms of attractive and repulsive forces and correlate it to imaging stability. Wang^{45,46} has applied the Krylov–Bogoliubov–Mitropolsky asymptotic approximation to predict the bistable amplitude response and compare the predictions to experiments (Fig. 4a). Nony *et al.*²³ and Boisgard *et al.*⁴⁷ have used a variational principle of least action to explain the hysteresis in amplitude-distance curves. García and San Paulo^{35,48–50} have demonstrated by numerical simulation the coexistence of two stable oscillations states in AM-AFM, the large amplitude state is termed the *net repulsive regime*, while the lower amplitude state is called the *attractive regime*. An investigation of the bifurcations and stability of the oscillations in AM-AFM have been performed by Rützel *et al.*²⁹, Lee *et al.*^{30,51}, and later by Yagasaki⁵². This bistable oscillatory behavior has elicited tremendous interest since it directly correlates to imaging instabilities. For instance, bistable behavior creates the possibility that the cantilever amplitude is identical at two different stand-off distances from the sample. This can lead to the feedback controller 'hunting' between these two stand-off distances to maintain constant amplitude, thus creating serious imaging artifacts^{48,49}.

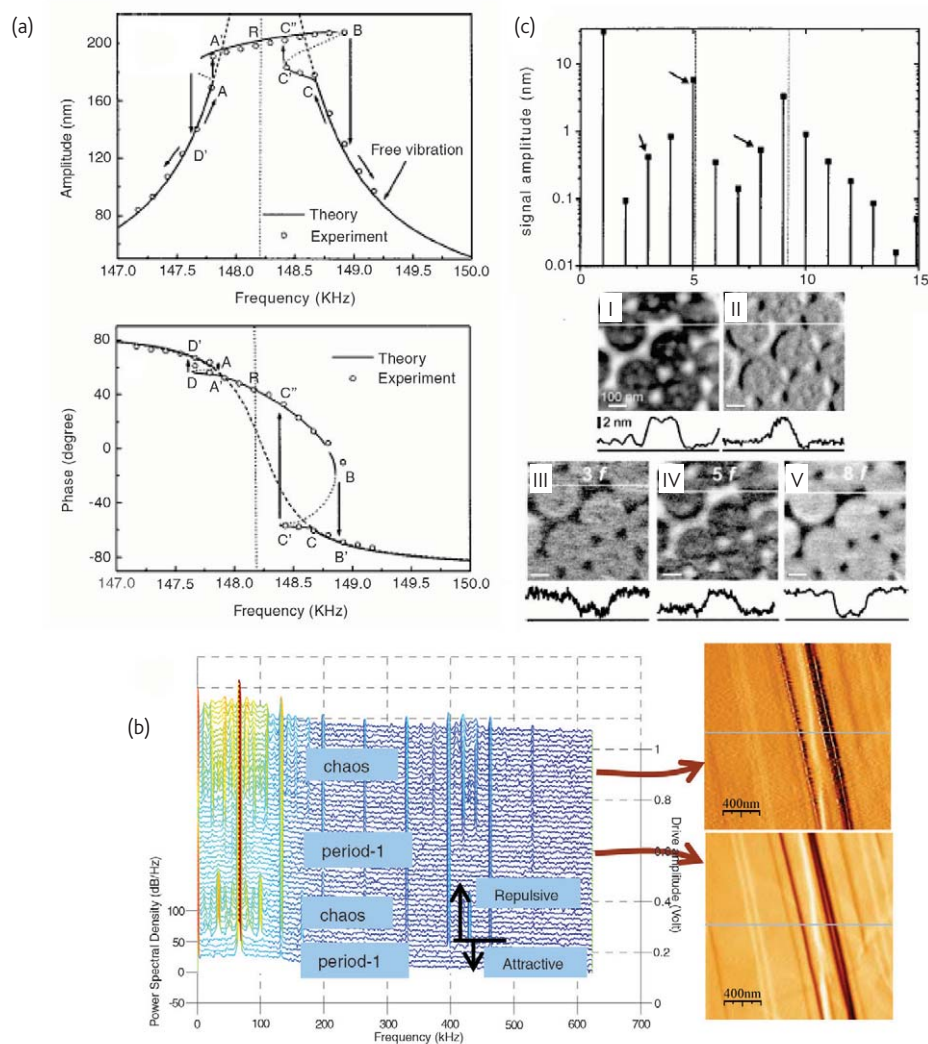


Fig. 4 Nonlinear dynamic phenomena in dAFM. (a) The coexistence of two stable oscillating states (one in the net repulsive and the other in the attractive regime) can be seen while keeping an AFM probe close to a surface and sweeping the drive frequency up and down across resonance. Tip amplitude and phase of oscillation are plotted⁴⁵. Solid black curves are the theoretically predicted stable response; dashed lines are unstable solutions; open circles are experimentally measured data using a stiff 40 Nm^{-1} Si cantilever on a polyethylene sample. (b) Chaotic oscillations of soft Si cantilevers on a graphite substrate set in during transition from the attractive to repulsive regimes of oscillation and then again at low setpoint ratios. Power spectra of the cantilever vibration are shown when the B1 mode is excited near the surface and the setpoint amplitude is decreased by increasing the drive voltage. Chaotic spectra are characterized by subharmonic peaks and broadband 'noise' below 150 kHz. Insets show error maps taken of a graphite substrate when the tip is oscillating periodically and chaotically, indicating that chaotic dynamics can introduce small but measurable uncertainty in nanometrology⁶⁴. (c) Theoretical simulations⁷⁶ showing the higher harmonics expected in the vibration frequency spectrum when a 52 kHz rectangular Si cantilever taps on a fused silica sample. Also shown below are images taken using multiple higher harmonics in air of a Pt-C layer on a fused silica cover slip SiO₂ grating. Clearly the higher harmonic images provide additional material contrast beyond what is observed in the topography image. (Reproduced with permission from^{45,64,76}. © 1998 American Institute of Physics, 2006 and 2005 American Physical Society, respectively.)

In AM-AFM, it is also possible under some circumstances for the cantilever to undergo chaotic oscillations. Ashhab *et al.*^{53,54} and Basso *et al.*⁵⁵ have used Melnikov theory to predict the existence of homoclinic chaos in a point-mass model of the AFM cantilever. Homoclinic chaos refers to a mechanism of chaos that can occur in a single-degree-of-freedom oscillator possessing one unstable equilibrium and two stable equilibria⁵⁶. More specifically, it can occur in an appropriate range of damping and excitation when a particle lies in a twin-well energy potential – a situation typically

observed when a soft cantilever is brought very close to a sample. The physical manifestation of this chaotic motion is that the tip chaotically switches between oscillating around two stable positions, one where the tip equilibrates under a small attractive force and another where it is 'stuck' to the sample. A more typical situation for AM-AFM is when the cantilever tip lies in a single-well potential and intermittently dynamically interacts with the sample. In contrast, van der Water and Molenaar⁵⁷, Hunt and Sarid⁵⁸, Berg and Briggs⁵⁹, and Dankowicz *et al.*⁶⁰ have all predicted the onset of subharmonic

motions and chaos in AM-AFM based on impact oscillator models of AM-AFM or using the theory of grazing bifurcations in nonsmooth systems. Sasaki *et al.*⁶¹ also theoretically predict the existence of quasiperiodic oscillations, as well as fractional resonances. Experimentally, both Burnham *et al.*⁶² and Salapaka *et al.*⁶³ have reported the observation of subharmonics and chaos-like motions in experiments where vibrating samples are made to impact a stationary cantilever. However, it has not been until recently^{64,65} that the onset of chaotic motion in AM-AFM has been systematically studied experimentally. It has been shown that chaotic oscillations set in for soft cantilevers when the tip initially transitions from the attractive to the repulsive regime of oscillation and then again when they are driven hard at low setpoint amplitudes (Fig. 4b)⁶⁴. The onset of chaotic motions in AFM cantilevers under realistic operating conditions can lead to small but measurable 'deterministic' uncertainty in nanoscale measurements.

Nonlinear dynamic phenomena have also provided many opportunities for improving sensitivity and material contrast. For example, it was observed early on that when a harmonically driven cantilever is brought in close proximity to a surface its harmonic motion is mixed with higher harmonic distortions because of nonlinear tip-sample interactions^{66,67}. Physically, the cantilever oscillates in the shape of its driven eigenmode but in time its oscillations contain higher harmonics. In principle, then, the higher harmonics contain detailed information about the tip-sample interaction potential. This idea has driven research and it is now reasonably well understood how the higher harmonics can be used to get information back out about the tip-sample interactions^{24,67-73}. Beyond the goal of the reconstruction of interaction forces (or force spectroscopy), it was quickly recognized that higher harmonics could also be used to enhance material contrast during imaging. By mapping the magnitudes of higher harmonics over a sample, it becomes possible to obtain sensitive material property contrasts for imaging in liquids^{66,74} and in air^{75,76} (Fig. 4c) and also to achieve subatomic contrast in low temperature AFM under ultrahigh vacuum (UHV) conditions⁷⁷.

In the absence of tip-sample nonlinear forces, the microcantilever eigenmodes are orthogonal to each other, meaning that the motion in each eigenmode can be considered independent of the motion in another eigenmode. However, in the presence of nonlinear tip-sample interaction forces, and when the natural frequencies of two different eigenmodes are close to the specific rational ratio of each other⁷⁸, it becomes possible for two eigenmodes to couple in the microcantilever response. This interesting nonlinear modal interaction phenomenon is also known as *internal resonance* in the nonlinear dynamics community⁷⁸. For example, Sahin *et al.*⁷⁹⁻⁸¹ and Balantekin and Atalar⁸² first demonstrated this theoretically and experimentally by fabricating cantilevers for which the B2 or T1 eigenmode frequencies are very close to an integer multiple of the B1 natural frequency. When such a cantilever is driven at a resonance of the B1 eigenmode

and brought close to the sample, some higher harmonics of the drive frequency are able to excite the B2 or T1 modes in a sensitive fashion. This then allows the sensitive measurement of nanomechanical properties using a specialized cantilever.

Another approach has been to excite the B1 and B2 eigenmodes of a cantilever simultaneously⁸³⁻⁸⁵. The nonlinear modal interactions between the two eigenmodes are such that the phase of the second eigenmode turns out to be very sensitive to variations in tip-sample interaction forces. Moreover, there is evidence that the attractive-repulsive bistability described earlier is significantly reduced when B1 and B2 are excited simultaneously⁸⁶. This *dual-mode* excitation method shows potential as a means of achieving high material contrast with gentle forces; however, the analytical and theoretical foundations of this method are not fully developed yet and remain a focus of current research.

Finally, a third category of nonconventional resonances used in dAFM is that of *parametric resonance*⁸⁷. Parametric resonance is a phenomenon that underlies the physics of swings and water waves. In order to achieve it in dAFM, the microcantilever stiffness needs to be modulated at a frequency nearly twice its natural resonance. This has been achieved by means of an electronic feedback circuit and an extremely sharp non-Lorentzian peak is obtained⁸⁷. Samples can be imaged at normal scan speeds without any ringing artifacts that are commonly associated with high *Q*-factor scans. The complete theoretical basis for this method is still under development.

Cantilever oscillations in liquids

As mentioned earlier, one of the most important and growing applications of AM-AFM is the imaging and nanomechanical measurements of soft biological matter in physiological buffer solutions. The potential of using AM-AFM in liquids was recognized in the early nineties and two important driving modes – the acoustic excitation mode^{88,89} and the magnetic mode⁹⁰ have been established. In the acoustic mode, vibrations of the dither piezo are transferred to the cantilever mechanically (structure-borne vibration), as well as indirectly through the fluid (fluid-borne vibration). In the magnetic mode, a cantilever with a magnetic film sputtered onto it is excited magnetically by a solenoid. The fundamental differences in cantilever dynamics between these two excitation modes are insignificant in air but become quite significant in liquids because of the low *Q*-factors of the cantilevers⁹¹⁻⁹³.

The surrounding liquid also serves to modify the 'wet' resonance frequency (cantilever resonance frequency in liquid) and *Q*-factor of resonance, especially when the cantilever is moved close to a sample surface. Predicting the hydrodynamics of cantilevers near a substrate has been a focus of many research groups and has been based broadly speaking on: (i) *ad hoc*, but intuitive, models⁹⁴; (ii) computational solutions using the boundary element method of the unsteady Stokes equations in two and three dimensions⁹⁵⁻⁹⁸; and (iii) transient, fully

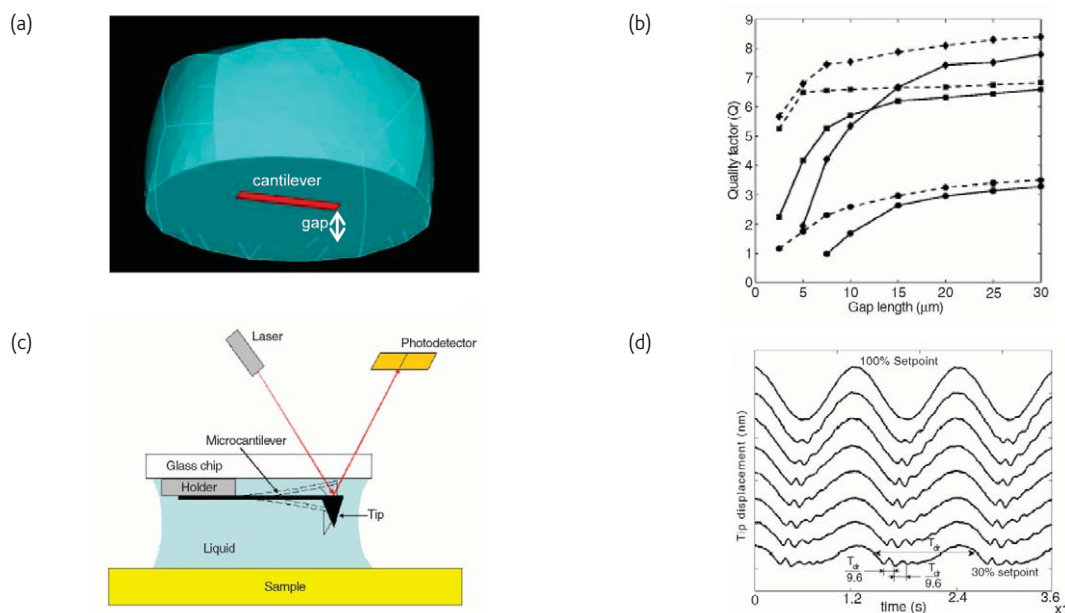


Fig. 5 Cantilever dynamics in liquids. (a) Computational three-dimensional flow-structure model of a rectangular Si cantilever ($197 \mu\text{m} \times 20 \mu\text{m} \times 2 \mu\text{m}$) close to a surface in water using the finite element code ADINA. (b) ADINA-computed Q -factors of B1 (circles), B2 (diamonds), and T1 (squares) modes⁹⁹ showing that the Q -factors (and wet resonance frequencies – not shown) decrease rapidly upon decrease of the gap. The rate of decrease depends on the mode number and the orientation of the cantilever (dashed lines are for a cantilever oriented at 11° to the sample surface), (c) when soft Si cantilevers are excited in the B1 eigenmode using magnetic excitation with an initial amplitude of $\sim 12 \text{ nm}$ and brought close to a mica sample in water¹⁰³ then (d) the tip oscillation waveform distorts significantly and often shows that the B2 mode is momentarily excited near tip-sample impact events. The significant harmonic waveform distortion in liquids while tapping samples is observed for both hard and soft samples and is characteristic of cantilever dynamics in liquid environments. (Reproduced with permission from^{99,103}. © 2006 and 2007 The American Institute of Physics, respectively.)

coupled fluid-structure interaction calculations using Navier–Stokes equations⁹⁹ (Fig. 5a). Broadly speaking, when a cantilever is brought close to a surface in a liquid medium, the Q -factors and wet resonance frequencies of the different eigenmodes decrease significantly (Fig. 5b). The rate of decrease with the gap depends strongly on the eigenmode of interest and also on the orientation of the cantilever relative to the surface (Fig. 5b).

While the dynamics of a microcantilever tapping on a sample is well understood under ambient or UHV conditions, the tip motion for AM-AFM in liquids has been studied to a lesser extent. Previous attempts at mathematical modeling of tip dynamics in liquids have used a Lennard–Jones type interaction potential^{66,100}, an exponentially growing force¹⁰¹, or a discontinuous interaction force¹⁰². In all cases it has been observed that, unlike in air, when a tip taps on a sample in liquids, significantly higher harmonics are generated and the tip motion distorts noticeably from a sine wave. More recently¹⁰³, it has been shown that the second bending mode plays a significant role in tip motion in liquids. Specifically, it has been shown that when a tip is excited in the B1 eigenmode and taps on a sample in a liquid medium, the B2 eigenmode is also excited momentarily at the point of tip-sample impact. All these studies are beginning to answer important questions about cantilever dynamics in liquid environments for AM-AFM applications. However, cantilever dynamics in liquids remain much less well understood than in air or vacuum.

Outlook

Two decades have passed since the invention of the AFM, but it has been only in the last eight years or so that a significant advance has taken place in understanding cantilever dynamics in dAFM. As a consequence of these studies, new imaging modes have emerged in the last two to three years that are based on a deep understanding of cantilever eigenmodes and nonlinear dynamics in dAFM. The dramatic improvements in imaging contrast or reduction in imaging forces afforded by these new modes are a worthy testament to the importance of cantilever dynamics in dAFM. Needless to say, the surface has only been scratched as far as the understanding of cantilever dynamics is concerned, especially under liquids.

The coming decade is likely to see further advances in the understanding of cantilever dynamics and a significant translation of technology toward the development of the next generation of AFMs. Based on the trends over the past years, it seems reasonable to assume that the greatest impact of cantilever dynamics in dAFM will lie in (i) applications to significantly improve the quantitative mechanical/electrical/magnetic property sensing using dAFM, (ii) applications for the development of new hydrodynamically streamlined AFM probes for applications in liquids, and (iii) the continued development of new modes for improved contrast with piconewton imaging forces for biological applications in liquids. 

REFERENCES

1. Binnig, G., et al., *Phys. Rev. Lett.* (1986) **56**, 930
2. Giessibl, F. J., *Rev. Mod. Phys.* (2003) **75**, 949
3. García, R., and Pérez, R., *Surf. Sci. Rep.* (2002) **47**, 197
4. Gleyzes, P., et al., *Appl. Phys. Lett.* (1991) **58**, 2989
5. Reinstädler, M., et al., *Surf. Sci.* (2003) **532**, 1152
6. Song, Y., and Bhushan, B., *Ultramicroscopy* (2006) **106**, 847
7. Sharos, L. B., et al., *Appl. Phys. Lett.* (2004) **84**, 4638
8. Reinstädler, M., et al., *Appl. Phys. Lett.* (2003) **82**, 2604
9. Reinstädler, M., et al., *J. Phys. D: Appl. Phys.* (2005) **38**, R269
10. Caron, A., et al., *Appl. Phys. Lett.* (2004) **85**, 6398
11. Kawagishi, T., et al., *Ultramicroscopy* (2002) **91**, 37
12. Huang, L., and Su, C., *Ultramicroscopy* (2004) **100**, 277
13. Sugimoto, Y., et al., *Appl. Phys. Lett.* (2007) **91**, 093120
14. Kawai, S., et al., *Appl. Phys. Lett.* (2005) **86**, 193107
15. Kawai, S., and Kawakatsu, H., *Appl. Phys. Lett.* (2006) **88**, 133103
16. Melcher, J., et al., *Appl. Phys. Lett.* (2007) **91**, 053101
17. Cappella, B., and Dietler, G., *Surf. Sci. Rep.* (1999) **34**, 1
18. Derjaguin, B. V., et al., *J. Colloid Interface Sci.* (1975) **53**, 314
19. San Paulo, A., and García, R., *Phys. Rev. B* (2001) **64**, 193411
20. Sarid, D., and Elings, V., *J. Vac. Sci. Technol. B* (1991) **9**, 431
21. Anczykowski, B., et al., *Phys. Rev. B* (1996) **53**, 15485
22. Sader, J. E., and Jarvis, S. P., *Appl. Phys. Lett.* (2004) **84**, 1801
23. Nony, L., et al., *J. Chem. Phys.* (1999) **111**, 1615
24. Stark, M., et al., *Proc. Natl. Acad. Sci. USA* (2002) **99**, 8473
25. Sader, J. E., et al., *Rev. Sci. Instrum.* (1995) **66**, 3789
26. Butt, H.-J., and Jaschke, M., *Nanotechnology* (1995) **6**, 1
27. Salapaka, M. V., et al., *J. Appl. Phys.* (1997) **81**, 2480
28. Rodríguez, T. R., and García, R., *Appl. Phys. Lett.* (2002) **80**, 1646
29. Rützel, S., et al., *Proc. R. Soc. London, Ser. A* (2003) **459**, 1925
30. Lee, S. I., et al., *Phys. Rev. B* (2002) **66**, 115409
31. Rast, S., et al., *Rev. Sci. Instrum.* (2000) **71**, 2772
32. Anczykowski, B., et al., *Appl. Surf. Sci.* (1999) **140**, 376
33. Giessibl, F. J., *Appl. Phys. Lett.* (2001) **78**, 123
34. Hu, S., and Raman, A., *Appl. Phys. Lett.* (2007) **91**, 123106
35. García, R., and San Paulo, A., *Phys. Rev. B* (1999) **60**, 4961
36. García, R., et al., *Phys. Rev. Lett.* (2006) **97**, 016103
37. Oyabu, N., et al., *Phys. Rev. Lett.* (2006) **96**, 106101
38. Zitzler, L., et al., *Phys. Rev. B* (2002) **66**, 155436
39. Sahagún, E., et al., *Phys. Rev. Lett.* (2007) **98**, 176106
40. Strus, M. C., et al., *Nanotechnology* (2005) **16**, 2482
41. Velegol, S. B., et al., *Langmuir* (2003) **19**, 851
42. Nony, L., et al., *Phys. Rev. B* (2006) **74**, 235439
43. Polesel-Maris, J., and Gauthier, S., *J. Appl. Phys.* (2005) **97**, 044902
44. Melcher, J., et al., *VEDA: Virtual Environment for Dynamic AFM*, (2007)
45. Wang, L., *Appl. Phys. Lett.* (1998) **73**, 3781
46. Wang, L. G., *Surf. Sci.* (1999) **429**, 178
47. Boisgard, R., et al., *Surf. Sci.* (1998) **401**, 199
48. García, R., and San Paulo, A., *Phys. Rev. B* (2000) **61**, 13381
49. San Paulo, A., and García, R., *Biophys. J.* (2000) **78**, 1599
50. San Paulo, A., and García, R., *Phys. Rev. B* (2002) **66**, 041406
51. Lee, S. I., et al., *Ultramicroscopy* (2003) **97**, 185
52. Yagasaki, K., *Phys. Rev. B* (2004) **70**, 245419
53. Ashhab, M., et al., *Nonlinear Dynam.* (1999) **20**, 197
54. Ashhab, M., et al., *Automatica* (1999) **35**, 1663
55. Basso, M., et al., *J. Dynam. Syst., Meas. Control* (2000) **122**, 240
56. Guckenheimer, J., and Holmes, P., *Nonlinear Oscillations, Dynamical Systems, and Bifurcations of Vector Fields*, Springer-Verlag, New York, (1983)
57. van de Water, W., and Molenaar, J., *Nanotechnology* (2000) **11**, 192
58. Hunt, J. P., and Sarid, D., *Appl. Phys. Lett.* (1998) **72**, 2969
59. Berg, J., and Briggs, G. A. D., *Phys. Rev. B* (1997) **55**, 14899
60. Dankowicz, H., et al., *Int. J. Non-Linear Mech.* (2007) **42**, 697
61. Sasaki, N., et al., *Appl. Phys. A* (1998) **66**, S287
62. Burnham, N. A., et al., *Phys. Rev. Lett.* (1995) **74**, 5092
63. Salapaka, S., et al., *Nonlinear Dynam.* (2001) **24**, 333
64. Hu, S., and Raman, A., *Phys. Rev. Lett.* (2006) **96**, 036107
65. Jamitzky, F., et al., *Nanotechnology* (2006) **17**, S213
66. van Noort, S. J. T., et al., *Langmuir* (1999) **15**, 7101
67. Dürig, U., *Appl. Phys. Lett.* (2000) **76**, 1203
68. Dürig, U., *New J. Phys.* (2000) **2**, 1
69. Hillenbrand, R., et al., *Appl. Phys. Lett.* (2000) **76**, 3478
70. Stark, M., et al., *Appl. Phys. Lett.* (2000) **77**, 3293
71. Stark, R. W., and Heckl, W. M., *Surf. Sci.* (2000) **457**, 219
72. Stark, R. W., *Nanotechnology* (2004) **15**, 347
73. Sebastian, A., et al., *IEEE Trans. Control. Syst. Technol.* (2007) **15**, 952
74. Preiner, J., et al., *Phys. Rev. Lett.* (2007) **99**, 046102
75. Stark, R. W., and Heckl, W. M., *Rev. Sci. Instrum.* (2003) **74**, 5111
76. Crittenden, S., et al., *Phys. Rev. B* (2005) **72**, 235422
77. Hembacher, S., et al., *Science* (2004) **305**, 380
78. Nayfeh, A. H., and Balachandran, B., *Applied Nonlinear dynamics: Analytical, Computational, and Experimental Methods*, John Wiley and Sons, New York, (1995)
79. Sahin, O., et al., *Phys. Rev. B* (2004) **69**, 165416
80. Sahin, O., et al., *Sens. Actuators A* (2004) **114**, 183
81. Sahin, O., et al., *Nat. Nanotechnol.* (2007) **2**, 507
82. Balantekin, M., and Atalar, A., *Appl. Phys. Lett.* (2005) **87**, 243513
83. Rodríguez, T. R., and García, R., *Appl. Phys. Lett.* (2004) **84**, 449
84. Martinez, N. F., et al., *Appl. Phys. Lett.* (2006) **89**, 153115
85. Proksch, R., *Appl. Phys. Lett.* (2006) **89**, 113121
86. Thota, P., et al., *Appl. Phys. Lett.* (2007) **91**, 093108
87. Moreno-Moreno, M., et al., *Appl. Phys. Lett.* (2006) **88**, 193108
88. Putman, C. A. J., et al., *Appl. Phys. Lett.* (1994) **64**, 2454
89. Schäffer, T. E., et al., *J. Appl. Phys.* (1996) **80**, 3622
90. Han, W., et al., *Appl. Phys. Lett.* (1996) **69**, 4111
91. Xu, X., and Raman, A., *J. Appl. Phys.* (2007) **102**, 034303
92. Kokavecz, J., and Mechler, A., *Appl. Phys. Lett.* (2007) **91**, 023113
93. Herruzo, E. T., and García, R., *Appl. Phys. Lett.* (2007) **91**, 143113
94. Rankl, C., et al., *Ultramicroscopy* (2004) **100**, 301
95. Green, C. P., and Sader, J. E., *Phys. Fluids* (2005) **17**, 073102
96. Green, C. P., and Sader, J. E., *J. Appl. Phys.* (2005) **98**, 114913
97. Clarke, R. J., et al., *J. Fluid Mech.* (2005) **545**, 397
98. Clarke, R. J., et al., *Proc. R. Soc. London, Ser. A* (2006) **462**, 913
99. Basak, S., et al., *J. Appl. Phys.* (2006) **99**, 114906
100. Sarid, D., et al., *Comput. Mater. Sci.* (1995) **3**, 475
101. Chen, G. Y., et al., *J. Vac. Sci. Technol. B* (1996) **14**, 1313
102. Legleiter, J., and Kowalewski, T., *Appl. Phys. Lett.* (2005) **87**, 163120
103. Basak, S., and Raman, A., *Appl. Phys. Lett.* (2007) **91**, 064107